CJC Chinese Journal of Chemistry 中国化学 - An International Journal

For submission: https://mc.manuscriptcentral.com/cjoc
For published articles: https://onlinelibrary.wiley.com/journal/16147065

Concise Report

Cite this paper: *Chin. J. Chem.* **2023**, *41*, 2648—2656. **DOI: 10.1002/cjoc.202300242**

Artemiprincepsolides A—F, Novel Germacrane-guaiane and Eudesmane-guaiane Sesquiterpenoid Dimers from *Artemisia princeps* and Their Antihepatoma Activity

Li-Hua Su,[a] Wen-Jing Ma,[a,b] Yun-Bao Ma,[a] Tian-Ze Li,[a] Chang-An Geng,[a] Wei Dong,[a,b] Xiao-Feng He,[a] Xue-Mei Zhang,[a] and Ji-Jun Chen*[,a,b]

[a] *State Key Laboratory of Phytochemistry and Plant Resources in West China, Kunming Institute of Botany, Chinese Academy of Sciences, Kunming, Yunnan 650201, China*
[b] *University of Chinese Academy of Sciences, Beijing 100049, China*

Keywords

Artemisia princeps | Hetero-coupled sesquiterpenoid dimers | Structure elucidation | Stereochemistry | Artemiprincepsolides | Biological activity | Antihepatoma activity | Apoptosis

Comprehensive Summary

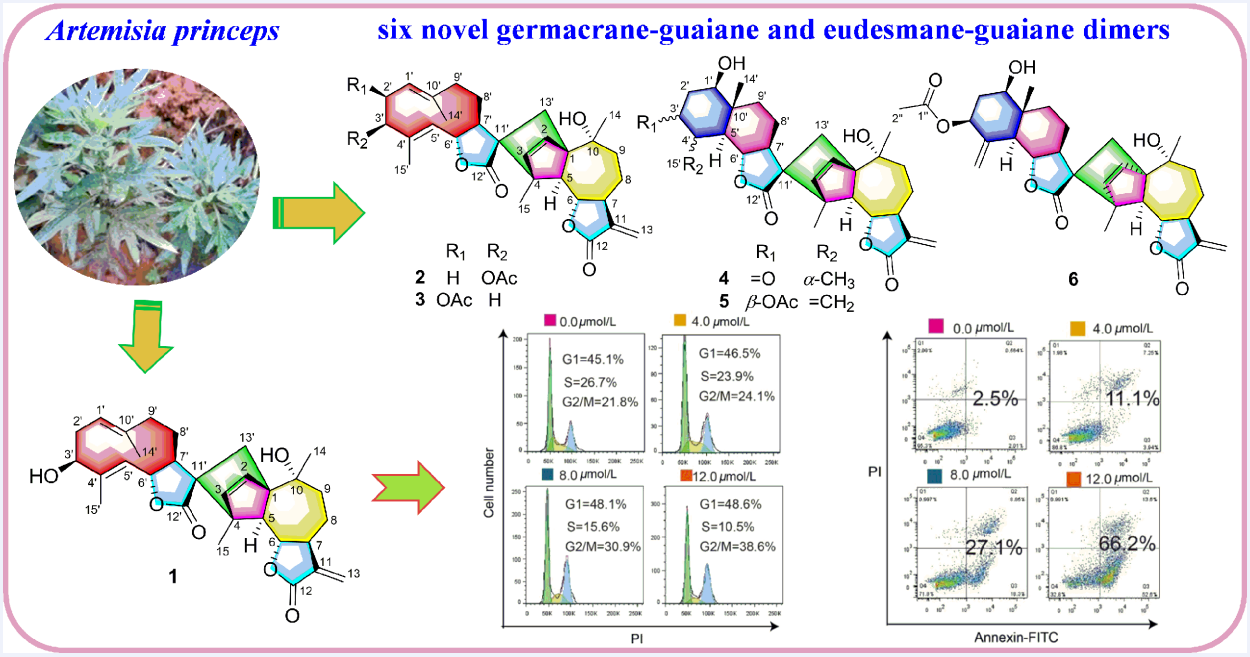

Artemiprincepsolides A—F (**1**—**6**) were isolated from *Artemisia princeps* guided by bioactivity and elucidated by comprehensive spectral data and ECD calculation. Compounds **1**—**3** represented the first connecting model of germacrane-guaiane hetero-dimeric adducts, and compounds **4**—**6** were eudesmane-guaiane hetero-coupled sesquiterpenoid dimers, meanwhile, all these were presumably formed by Diels-Alder cycloaddition. Compounds **1**—**6** were evaluated for their hepatomatic cytotoxicity on three hepatoma cell lines, and demonstrated cytotoxicity with IC_{50} values in the range of 5.0—67.3 μmol/L. Interestingly, compound **1** manifested significant cytotoxicity against HepG2, Huh7, and SK-Hep-1 cells with IC_{50} values of 9.9, 9.2, and 5.0 μmol/L, which were almost equivalent to the positive control, sorafenib. Flow cytometry data and Western blot assays revealed the most active compound **1** dose-dependently inhibited cell migration and invasion, and significantly induced HepG2 cells arrest in G2/M phase by downregulating proteins pcdc2 and upregulating the level of protein CyclinB1; and induced apoptosis by downregulating of Bcl-2 expression and upregulating Bax level.

*E-mail: chenjj@mail.kib.ac.cn

Background and Originality Content

Hepatocellular carcinoma (HCC) is the main form of liver cancer and difficult to achieve the optimum efficiency for the current clin. treatment methods.[1] Therefore, it is urgent to explore new and effective treatment strategies and therapeutic drugs. Although the incidence of HCC has reduced in some areas with the increased use of vaccines against HBV, the global incidence and mortality rates of HCC continue to increase.[2-4] Because the symptoms and physical features of HCC cannot be easily recognized, curative treatment is not possible at the time of diagnosis for >80% of patients. Thus, the treatment of HCC remains a major healthcare challenge globally, and novel diagnostic and treatment options for this fatal disease are urgently needed.[5-6] Natural products play a key role in antihepatoma and maintaining immunity, among which sesquiterpenoid dimers have become a main focus of medicinal and synthetic chemistry because of their fascinating structures and remarkable bioactivities.[7] Up to now, hundreds of dimeric sesquiterpenoids have been reported from various plants, animals and even sea creatures, and some of them have displayed important biological activities, such as anti-inflammatory, antitumor, antimalarial, and immunosuppressive effects.[8-12] Most of them are formed by Diels-Alder reaction, hetero-Diels–Alder, [2+2] cycloaddition, Michael addition, free-radical reaction, and aldol reaction.

Artemisia princeps (Asteraceae family) is a perennial herbaceous plant and widely distributed in East Asia. Its leaves are commonly used as tea, spices, and cooking ingredient, and have long been used as a folk traditional herbal medicine for the treatment of inflammation, hemostasis, pain, gastric ulcer, and circulatory disorders.[13-14] Previous phytochemical investigations on *A. princeps* revealed the existence of sesquiterpenoids, triterpenoids, steroids, flavonoids, coumarin, polyacetylenes, and some other components.[15-19] And the types of sesquiterpenoids from this species include eudesmane, guaiane, germacrane, humulane, caryophyllane, and himachalane.[20-22] However, none of the sesquiterpenoid dimers has been reported so far.

Our previous investigation on *A. atrovirens* and *A. dubia* reported 48 guaiane-type dimers through [4 + 2] Diels–Alder cyclization and six novel hetero-dimeric adducts dimerized from a rotundane-type unit and a guaiane-type monomer, and three pseudo dimers were linked though an ester bond, and demonstrated 50 compounds with cytotoxicity against HepG2, SMMC-7721, Huh7, and SK-Hep-1 cell lines with IC_{50} values in the range of 3.3 to 257.6 μmol/L.[23-26] Preliminary mechanism study manifested that lavandiolide H dose-dependently inhibited cell migration and invasion, induced G2/M cell cycle arrest and cell apoptosis in HepG2 cells by downregulating the expression of Bcl-2 and PARP-1, and activating PARP-1 to up-regulate the expression of cleaved-PARP-1;[23] artematrolide A showed significant cytotoxic activity against HeLa S3 and SiHa cells by activating ROS/ERK/mTOR signaling pathway and promoting metabolic shift.[27] Artemidubolide D dose-dependently inhibited cell migration and invasion, induced G1 cell cycle arrest by downregulating proteins CDK4, CDK6 and CyclinD1 and upregulating the level of protein P21, and induced apoptosis by downregulating of PARP-1 and Bcl-2 expression and upregulating Bax and cleaved PARP-1 levels.[26] Very recently, 36 novel sesquiterpenoid dimers were isolated from *A. eriopoda*. Functional experiments showed that artemeriopodin G7 could inhibit cell migration and invasion, induce G2/M cell cycle arrest and cell apoptosis, upregulate PDGFRA expression, and dramatically suppress the activity of AKT/STAT signaling pathway by downregulating the expression of phosphorylated AKT/STAT.[28]

In this study, as one of the further investigations to search new antihepatoma sesquiterpenoid dimers from the same genus species, bioactivity-guided fractionation was performed on the ethanol extract of stems and leaves of *A. princeps* to provide six novel hetero-dimeric [4+2] adducts, artemiprincepsolides A—F (**1**—**6**) (Figure 1). This paper described the details of the isolation, structural elucidation, and biological assays of compounds **1**—**6**, and a preliminary mechanism for compound **1** in HepG2 cells was presented.

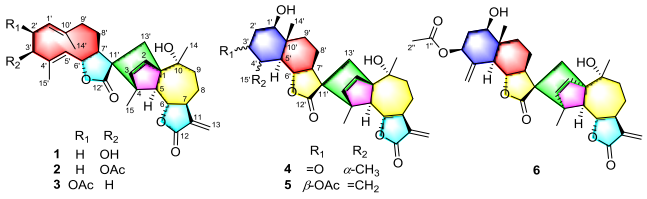

Figure 1 Chemical structures of artemiprincepsolides A—F (**1**—**6**).

Results and Discussion

Artemiprincepsolide A (**1**) was obtained as white amorphous powder and had a molecular formula of $C_{30}H_{38}O_6$ with 12 double bond equivalents deduced from the (–)-HRESIMS data at *m/z* 539.2659 ($[M + HCOO]^-$, calcd for $C_{31}H_{39}O_8$, 539.2650). Its IR spectrum exhibited absorption bands at 3495, 1764, 1712, and 1632 cm^{-1}, indicating the existence of hydroxy, carbonyl, and olefinic functionalities. The ^1H NMR spectrum (Table 1) of compound **1** displayed four singlet methyls at δ_H 1.35 (3H, s), 1.42 (3H, s), 1.45 (3H, s), and 1.70 (3H, s), three oxygenated methines at δ_H 4.19 (1H, dd, *J* = 9.9, 9.6 Hz), δ_H 4.27 (1H, br s), and δ_H 4.55 (1H, dd, *J* = 9.9, 9.6 Hz), four olefinic protons at δ_H 4.69 (1H, d, *J* = 9.6 Hz), 4.89 (1H, br d, *J* = 10.8 Hz), 5.94 (1H, d, *J* = 5.7 Hz), 6.29 (1H, d, *J* = 5.7 Hz), and one exocyclic methylene group at δ_H 5.38 (1H, d, *J* = 3.3 Hz) and 6.11 (1H, d, *J* = 3.3 Hz). Its ^{13}C NMR spectrum (Table 2) exhibited 30 carbon resonances classified as four methyls, seven methylenes (one olefinic carbon), ten methines (two oxygenated and four olefinic carbons), and nine nonprotonated carbons (one oxygenated and three olefinic carbons). The abovementioned NMR and LC-MS-IT-TOF data suggested compound **1** should be a sesquiterpenoid dimer derived from two hetero sesquiterpenoid units.

The planar skeleton of compound **1** was determined by detailed analysis of the 2D NMR (^1H–^1H COSY and HMBC) data (Figure 2). The ^1H–^1H COSY correlations of H-2/H-3 and H-5/H-6/H-7/H_2-8/H_2-9, along with the HMBC correlations from H-2 to C-1, and C-10, from H_2-13 to C-7, C-11, and C-12, from H_3-14 to C-1, C-9, and C-10, and from H_3-15 to C-3, C-4, and C-5, established guaianolide unit (unit A). As for the remained NMR signals, the spin systems of H-1′/H_2-2′/H-3′ and H-5′/H-6′/H-7′/H_2-8′/H_2-9′ in ^1H–^1H COSY correlations, together with the cross peaks from H-7′ to C-11′, C-12′, and C-13′, from H_3-14′ to C-1′, C-9′, and C-10′, from H_3-15′ to C-3′, C-4′, and C-5′ in the HMBC spectrum revealed a germacranolide unit (unit B). Furthermore, the connection of units A and B through two C—C bonds of C-1–C-13′ and C-4–C-11′ was established by the key correlations of H-2 with C-13′, of H-7′ with C-4, and of H_3-15 with C-11′ in the HMBC spectrum. Hence, the planar structure of compound **1** was finalized.

The relative configuration of compound **1** was determined by interpretation of ROESY spectrum (Figure 3) and coupling constants. The configuration of H-7 in guaianolides with an *α*-methylene-*γ*-lactone group could be defined as *α*-orientation according to the Geissmann rule.[26,29-30] The large coupling constant between H-6 and H-7 ($J_{6,7}$ = 9.6 Hz) indicated their *trans* spatial relationship, and H-6 was confirmed to be *β*-orientated. In the ROESY spectrum, the cross peaks of H-7/H-5, H-5/H_3-15, H-6/H-2, H-6/H-3, and H-2/H_3-14 suggested the *β*-orientation of vinyl (C-2–C-3) and CH_3-14, and the *α*-orientation of H-5 and CH_3-15. In unit B, the large coupling constant between H-6′ and H-7′ ($J_{6',7'}$ = 9.6 Hz) indicated H-6′ was *β*-orientated. In the ROESY spectrum, the cross peaks of H-7′/H-3′, H-7′/H_2-13′ suggested the *α*-orientation of H-3′and CH_2-13′. Furthermore, the H-3′ was

Table 1 ^{1}H NMR data for compounds **1**—**6** in $CDCl_3$ (600 MHz, *J* in Hz)

No.	1	2	3	4	5	6
2	5.94 (d, 5.7)	5.93 (d, 5.4)	5.93 (d, 5.4)	5.91 (d, 5.7)	5.90 (d, 5.4)	6.00 (d, 6.0)
3	6.29 (d, 5.7)	6.27 (d, 5.4)	6.30 (d, 5.4)	6.31 (d, 5.7)	6.31 (d, 5.4)	5.89 (d, 6.0)
5	2.37 (d, 9.9)	2.35 (d, 9.6)	2.24 (d, 10.2)	2.12 (d, 9.9)	2.11 (ol)	3.12 (d, 10.2)
6	4.19 (dd, 9.9, 9.6)	4.19 (dd, 9.6, 9.6)	4.18 (dd, 10.2, 10.2)	4.17 (dd, 9.9, 9.6)	4.18 (m)	4.06 (dd, 10.2, 9.6)
7	3.22 (m)	3.21 (m)	3.20 (m)	3.22 (m)	3.22 (m)	3.35 (m)
8	2.23 (m)	2.22 (m)	2.21 (m)	2.23 (m)	2.22 (ol)	2.26 (m)
	1.51 (ol)	1.50 (ol)	1.49 (ol)	1.51 (m)	1.50 (m)	1.43 (ol)
9	1.93 (m)	1.93 (m)	1.90 (m)	1.93 (m)	1.91 (m)	1.87 (m)
	1.85 (m)	1.86 (m)	1.83 (m)	1.86 (m)	1.85 (ol)	1.84 (ol)
13	6.11 (d, 3.3)	6.11 (d, 3.3)	6.09 (d, 3.6)	6.11 (d, 3.0)	6.10 (d, 3.3)	6.09 (d, 3.6)
	5.38 (d, 3.3)	5.37 (d, 3.3)	5.35 (d, 3.6)	5.37 (d, 3.0)	5.37 (d, 3.3)	5.36 (d, 3.6)
14	1.35 (s)	1.34 (s)	1.33 (s)	1.35 (s)	1.35 (s)	1.31 (s)
15	1.42 (s)	1.41 (s)	1.40 (s)	1.37 (s)	1.37 (s)	1.58 (ol)
1'	4.89 (br d, 10.8)	4.91 (dd, 13.2, 4.2)	5.06 (d, 8.3)	3.67 (dd, 11.9, 5.6)	3.61 (m)	3.55 (m)
2'	2.46 (m)	2.52 (m)	5.78 (m)	2.74 (dd, 15.3, 5.6)	2.22 (ol)	2.20 (m)
	2.26 (m)	2.29 (ol)		2.54 (dd, 15.3, 11.9)	1.60 (m)	1.59 (ol)
3'	4.27 (br s)	5.17 (dd, 10.8, 6.0)	2.69 (m)		5.17 (m)	5.14 (dd, 11.9, 5.6)
			2.30 (br d, 14.0)			
4'				2.47 (m)		
5'	4.69 (d, 9.6)	4.78 (d, 9.9)	4.85 (d, 10.2)	1.44 (ol)	2.02 (d, 10.2)	1.84 (ol)
6'	4.55 (dd, 9.6, 9.6)	4.51 (dd, 9.9, 9.0)	4.47 (dd, 10.2, 10.2)	4.04 (dd, 10.8, 10.2)	4.15 (m)	4.47 (dd, 10.8, 10.8)
7'	2.28 (m)	2.29 (ol)	2.17 (m)	2.21 (m)	2.22 (ol)	1.97 (m)
8'	2.15 (m)	2.15 (m)	2.26 (m)	1.88 (m)	1.84 (ol)	1.72 (m)
	1.58 (m)	1.58 (m)	1.31 (m)	1.78 (m)	1.72 (m)	1.43 (ol)
9'	2.44 (ol)	2.43 (ol)	2.44 (m)	2.17 (m)	2.08 (m)	2.04 (m)
	2.05 (m)	2.07 (m)	1.67 (m)	1.32 (m)	1.33 (m)	1.12 (m)
13'	2.44 (ol)	2.43 (ol)	2.37 (d, 12.0)	2.36 (d, 11.4)	2.37 (d, 11.4)	2.61 (d, 11.7)
	1.51 (ol)	1.50 (ol)	1.48 (ol)	1.45 (ol)	1.47 (m)	1.27 (d, 11.7)
14'	1.45 (s)	1.46 (s)	1.75 (s)	1.12 (s)	0.84 (s)	0.85 (s)
15'	1.70 (s)	1.66 (s)	1.73 (s)	1.24 (d, 6.6)	5.16 (br s)	5.18 (br s)
					4.91 (br s)	4.99 (br s)
2''		2.09 (s)	2.06 (s)		2.12 (s)	2.14 (s)

''ol'' is used to indicate overlapped signals, for which the coupling constants could not be read.

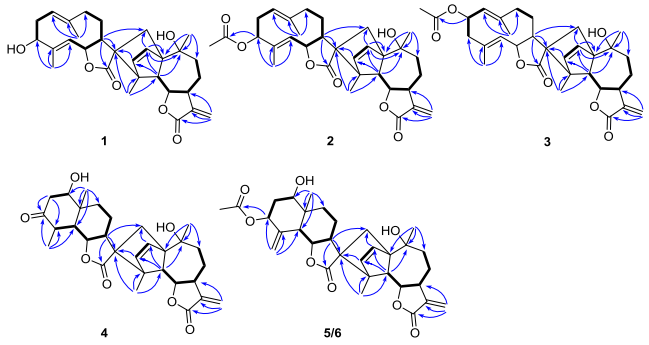

Figure 2 ^{1}H–^{1}H COSY (—) and key HMBC (→) correlations of compounds **1**—**6**.

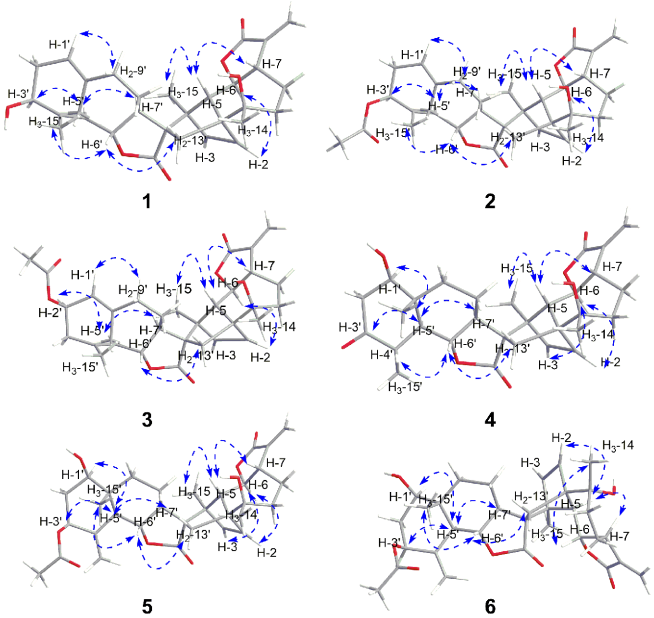

Figure 3 Key ROESY correlations of compounds **1**—**6**.

assigned an *α*-orientation which was inferred by the chemical shifts of the monomeric germacranolide hanphyllin.[31]

Furthermore, the ROESY correlations of H-1′/H_2-9′ and H-6′/H_3-15′ suggested the *E* geometry of $\Delta^{1',10'}$ and $\Delta^{4',5'}$ double bonds. The absolute configuration of compound **1** was defined as 1*R*,4*R*,5*S*,6*S*,7*S*,10*R*,3′*S*,6′*R*,7′*S*,11′*R* by TDDFT quantum calculation, in which the calculated ECD spectrum matched well with the experimental spectrum (Figure 4).

Artemiprincepsolides B (**2**) and C (**3**) showed same molecular formulas of $C_{32}H_{40}O_7$ as established from their (–)-HRESIMS data at *m*/*z* 581.2734 ([M + HCOO]$^-$, calcd 581.2756) and 581.2751 ([M + HCOO]$^-$, calcd 581.2756), respectively. Compound **2** showed highly similar NMR data with those of **1**, except that C-3' in **2** was substituted by an acetoxy group, which was supported by the

Table 2 ^{13}C NMR data for compounds **1**—**6** in $CDCl_3$ (150 MHz)

No.	1	2	3	4	5	6
1	64.4 C	64.4 C	64.8 C	63.8 C	63.8 C	63.0 C
2	133.7 CH	133.8 CH	134.0 CH	133.6 CH	133.6 CH	136.9 CH
3	141.5 CH	141.4 CH	141.0 CH	141.0 CH	140.9 CH	137.7 CH
4	59.4 C	59.4 C	58.9 C	57.3 C	57.2 C	60.7 C
5	66.5 CH	66.5 CH	65.8 CH	66.9 CH	66.9 CH	66.9 CH
6	80.0 CH	79.9 CH	79.8 CH	79.8 CH	79.8 CH	79.6 CH
7	43.6 CH	43.6 CH	43.5 CH	43.6 CH	43.6 CH	43.3 CH
8	23.6 CH_2	23.6 CH_2	23.6 CH_2	23.6 CH_2	23.6 CH_2	23.9 CH_2
9	35.3 CH_2	35.2 CH_2	35.2 CH_2	35.1 CH_2	35.1 CH_2	34.8 CH_2
10	73.5 C	73.4 C	73.3 C	73.3 C	73.2 C	72.7 C
11	141.0 C	141.0 C	141.2 C	140.9 C	141.0 C	141.0 C
12	170.8 C	170.8 C	170.7 C	170.9 C	170.9 C	170.7 C
13	119.0 CH_2	118.9 CH_2	118.9 CH_2	119.0 CH_2	119.0 CH_2	118.9 CH_2
14	30.2 CH_3	30.2 CH_3	30.0 CH_3	30.2 CH_3	30.1 CH_3	30.0 CH_3
15	15.6 CH_3	15.5 CH_3	15.9 CH_3	15.3 CH_3	15.3 CH_3	17.2 CH_3
1'	125.2 CH	124.2 CH	126.0 CH	76.2 CH	75.8 CH	76.0 CH
2'	35.3 CH_2	32.1 CH_2	71.6 CH	46.5 CH_2	37.1 CH_2	37.2 CH_2
3'	78.4 CH	79.2 CH	45.0 CH_2	208.5 C	70.5 CH	70.5 CH
4'	141.2 C	137.2 C	138.8 C	45.1 CH	140.8 C	140.6 C
5'	125.3 CH	126.7 CH	127.0 CH	49.9 CH	50.0 CH	51.5 CH
6'	78.8 CH	78.5 CH	79.1 CH	79.8 CH	75.6 CH	77.1 CH
7'	51.3 CH	51.2 CH	49.2 CH	50.9 CH	49.9 CH	55.2 CH
8'	27.4 CH_2	27.4 CH_2	31.1 CH_2	21.4 CH_2	21.6 CH_2	22.7 CH_2
9'	41.1 CH_2	41.1 CH_2	35.6 CH_2	36.1 CH_2	35.7 CH_2	37.1 CH_2
10'	137.9 C	138.9, C	137.9 C	41.2 C	42.0 C	42.5 C
11'	57.4 C	57.3 C	57.2 C	56.5 C	57.3 C	56.6 C
12'	179.4 C	179.3 C	179.6 C	178.8 C	179.0 C	181.4 C
13'	36.7 CH_2	36.7 CH_2	36.4 CH_2	35.4 CH_2	35.5 CH_2	42.8 CH_2
14'	16.7 CH_3	16.7 CH_3	22.6 CH_3	11.9 CH_3	11.6 CH_3	11.9 CH_3
15'	11.9 CH_3	12.5 CH_3	18.9 CH_3	14.1 CH_3	107.8 CH_2	108.1 CH_2
1''		170.2 C	170.5 C		169.8 C	170.0 C
2''		21.2 CH_3	21.4 CH_3		21.1 CH_3	21.2 CH_3

correlations between H-3' (δ_H 5.17, dd, J = 10.8, 6.0 Hz) and C-1'' (δ_C 170.2) in the HMBC spectrum. And compound **3** differed from **2** only in the location of an acetoxyl group, which was confirmed by the key HMBC correlation from H-2' (δ_H 5.78, m) to C-1'' (δ_C 170.5), and the H-1'/H-2'/H_2-3' correlations in the ^1H–^1H COSY spectrum. Careful analysis of the ROESY spectrum (Figure 3) and the coupling constants indicated compound **2** had the same configuration as **1**, and compound **3** shared the same stereochemistry as **1** at all chiral centers except for C-2'. The relative configuration of C-2' in **3** was mainly deduced from ROESY correlations of H-7'/H-9'b and H-9'b/H-2'. Therefore, their absolute stereochemistry was determined as 1*R*,4*R*,5*S*,6*S*,7*S*,10*R*,3'*S*,6'*R*,7'*S*,11'*R* for **2** and 1*R*,4*R*,5*S*,6*S*,7*S*,10*R*,3'*S*,6'*R*,7'*S*,11'*R* for **3** by comparing the calculated and experimental ECD spectra (Figure 4).

Artemiprincepsolide D (**4**), a white amorphous powder, was assigned the molecular formula of $C_{30}H_{38}O_7$ based on its (–)-HRESIMS data at m/z 555.2606 ($[M + HCOO]^-$, calcd 555.2600), corresponding to 12 degrees of unsaturation. The IR spectrum manifested the presence of hydroxy (3447 cm^{-1}), carbonyl (1766 and 1714 cm^{-1}) and olefinic (1643 cm^{-1}) groups. Thirty carbons were observed in the ^{13}C NMR spectrum, combination with the characteristic NMR signals for an eudesmane-type moiety and a guaianolide unit, revealing that compound **4** was also a heterodimeric sesquiterpenoid. The ^1H–^1H COSY spectrum showed four isolated spin-coupling systems of H-2/H-3, H-5/H-6/H-7/H_2-8/H_2-9, H-1'/H_2-2', and H-4'/H-5'(H_3-15')/H-6'/H-7'/H_2-8'/H_2-9'. In the HMBC spectrum, the cross peaks from H-2 to C-4, C-5, and C-10, from H-8 to C-6, C-10, and C-11, from H_2-13 to C-7, C-11, and C-12, from H_3-14 to C-1, C-9, and C-10, and from H_3-15 to C-3, C-4, and C-5 constructed unit A; and the correlations from H_3-14' to C-1', C-9', and C-10', from H_3-15' to C-3', C-4', and C-5', from H-7' to C-5', C-6', C-8', C-9', C-12', and C-13', and from H_2-13' to C-7', C-11', and C-12') constructed unit B. Furthermore, the cross peaks from H_3-15 to C-11', from H-3 to C-11', from H-5 to C-11', and from H_2-13' to C-1, C-2, and C-10 in the HMBC spectrum further confirmed the connecting model of compound **4**, which is the same as compound **1**. Hence, the planar structure of **4** was established.

The relative configuration of compound **4** was determined from its ROESY spectrum (Figure 3). The configuration of CH_3-14' might be defined as *β*-orientation based on the fact that most reported eudesmanolids from the genus *Artemisia* were found to possess the same characteristic.[32-34] In the ROESY spectrum, the correlations of H-7/H-5, H-5/H_3-15, H-7'/H-5', H-7'/H_2-13', H-5'/H_3-15', and H-5'/H-1' suggested the *α*-orientation of H-5, H-5', H-1', CH_3-15', and CH_2-13'. While the ROESY correlations of H-6/H-2, H-6/H-3, H-6/H_3-14, H-6'/H_3-14' indicated the *β*-orientation of CH_3-14, CH_3-14' and the vinyl (C-2–C-3). The absolute configuration of compound **4** was deduced to be 1*R*,4*R*,5*S*,6*S*,7*S*,10*R*,1'*R*,4'*S*,5'*S*,6'*S*,7'*S*,10'*R*,11'*R* by a comparison of the experimental ECD spectrum with the calculated one (Figure 4).

Artemiprincepsolide E (**5**) possessed a molecular formula of $C_{32}H_{40}O_8$ as deduced from the (–)-HRESIMS ion at m/z 597.2491 $[M + HCOO]^-$ (calcd for $C_{33}H_{41}O_{10}$, 597.2494). The presence of hydroxyl (3468 cm^{-1}), carbonyl (1754 cm^{-1}), and olefinic (1631 cm^{-1}) functionalities was evident from the IR spectrum. The ^1H and ^{13}C NMR data (Tables 1 and 2) of compound **5** were similar to those of

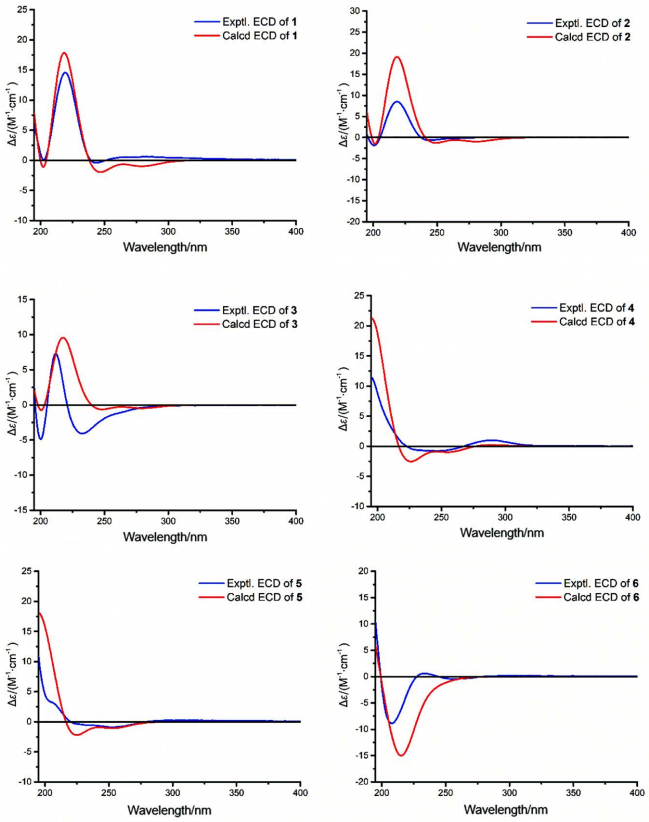

Figure 4 The experimental and calculated ECD spectra of compounds **1**—**6**.

compound **4**, and the main difference was that a keto-carbonyl at C-3' and a doublet methyl at C-4' in compound **4** were replaced by an oxygenated methine (δ_C 70.5) and the terminal olefinic carbon (δ_C 107.8 and 140.8) in compound **5**. Meanwhile, the presence of an acetoxy group at δ_H 2.12 (s, H_3-2'') and δ_C 21.1 (C-2''), 169.8 (C-1'') was observed in compound **5**. The above deduction was confirmed by the ^{1}H–^{1}H COSY correlations of H_2-2'/H-3' and HMBC cross peaks from H_2-15' to C-3', C-4', and C-5', and from H-3' to C-1''.

In the ROESY spectrum, the cross peaks of H-7/H-5, H-5/H_3-15, H-7'/H-5', H-7'/H_2-13', H-5'/H-1', and H-5'/H-3' revealed H-5, CH_3-15, H-1', H-3', H-5', and CH_2-13' were α-oriented, while the correlations of H-6/H_3-14, H-6/H-2, H-6/H-3, H-6'/H_3-14' indicated CH_3-14, CH_3-14' and the vinyl (C-2–C-3) were β-oriented. The calculated ECD spectrum of compound **5** matched well with the experimental one (Figure 4), confirming the absolute configuration as 1*R*,4*R*,5*S*,6*S*,7*S*,10*R*,1'*R*,3'*S*,5'*S*,6'*S*,7'*S*,10'*R*,11'*R*.

Artemiprincepsolide F (**6**) possessed a molecular formula of $C_{32}H_{40}O_8$ as determined by the (–)-HRESIMS ion at *m*/*z* 597.2708 $[M + HCOO]^-$ (calcd for $C_{33}H_{41}O_{10}$, 597.2705), which is identical to those of compound **5**. The IR spectrum manifested the presence of hydroxy (3435 cm^{-1}), carbonyl (1763 cm^{-1}) and olefinic (1631 cm^{-1}) functional groups. Interpretation of the ^{1}H and ^{13}C NMR spectra (Tables 1 and 2) indicated that compound **6** possessed the same planar structure as compound **5**, and the major difference was the chemical shifts of C-2 at δ_C 136.9, C-3 at δ_C 137.7, C-4 at δ_C 60.7, C-15 at δ_C 17.2, and C-13' at δ_C 42.8 for compound **6** in contrast to δ_C 133.6, 140.9, 57.2, 15.3, and 35.5 for compound **5**, which indicated compound **6** was a diastereoisomer of **5**. In the ROESY spectrum (Figure 3), the cross peaks of H-7/H-5, H-5/H-2, H-5/H-3, H-7'/H-5', H-5'/H-1', and H-5'/H-3' indicated the α-configuration of H-5, vinyl (C-2–C-3), H-5', H-1', and H-3', while the correlations of H-6/H_3-14, H-6'/H_3-14', and H-6'/H_2-13' revealed that CH_3-14, CH_3-14', and CH_2-13' were β-oriented. Its absolute stereochemistry was assigned to be 1*S*,4*S*,5*S*,6*S*,7*S*,10*R*,1'*R*,3'*S*,5'*S*,6'*S*,7'*S*,10'*R*,11'*R* by the high agreement between the experimental and calculated ECD spectra (Figure 4).

The EtOH extract and EtOAc fraction of *A. princeps* were tested for their inhibitory activity on three hepatoma cell lines with inhibitory ratios of 33.9%, 87.9% (HepG2), 55.1%, 88.3% (Huh7), and 82.0%, 101.2% (SK-Hep-1) at 200.0 μg/mL (Table S1). The EtOAc fraction was separated into five subfractions (Fr. 1—Fr. 5), of which Fr. 2 and Fr. 3 showed obvious cytotoxicity with the inhibitory ratios of 94.2%, 94.6% (HepG2), 89.7%, 92.1% (Huh7), and 90.3%, 93.8% (SK-Hep-1), more potent than three other subfractions at 200.0 μg/mL.

The obtained novel hetero-dimers (**1**—**6**) from Fr. 2 and Fr. 3 were evaluated cytotoxicity against HepG2, Huh7, and SK-Hep-1 cell lines and the results are shown in Table 3. As for HepG2 cells, compounds **1**—**3** exhibited cytotoxicity with IC_{50} values of 9.9, 26.4, and 24.9 μmol/L, while compounds **4**—**6** showed moderate cytotoxic activity with IC_{50} values of 41.0, 46.2, and 65.8 μmol/L. Compounds **1**, **3**, and **5** displayed cytotoxicity with IC_{50} values of 9.2, 20.1, and 24.6 μmol/L in Huh7 cells. Compounds **1**—**4** manifested cytotoxicity with IC_{50} values of 5.0, 18.8, 19.7, and 28.1 μmol/L in SK-Hep-1 cells. Interestingly, compound **1** manifested obvious cytotoxicity against three human hepatoma cell lines with IC_{50} values of 9.9, 9.2, and 5.0 μmol/L, which were superior to those of sorafenib (IC_{50} 10.8, 11.0, 8.4 μmol/L).

Table 3 Cytotoxicity of compounds **1**—**6** from *A. princeps*

Compound	IC_{50}[a]/(μmol·L^{-1})		
	HepG2	Huh7	SK-Hep-1
1	9.9 ± 0.2	9.2 ± 0.1	5.0 ± 0.6
2	26.4 ± 0.6	30.9 ± 0.5	18.8 ± 0.7
3	24.9 ± 1.0	20.1 ± 0.2	19.7 ± 0.3
4	41.0± 2.1	32.1 ± 0.6	28.1 ± 0.5
5	46.2 ± 2.8	24.6 ± 0.9	43.6 ± 1.5
6	65.8 ± 2.3	67.3 ± 0.2	35.5 ± 2.2
Sorafenib[b]	10.8 ± 0.1	11.0 ± 1.2	8.4 ± 0.1

[a] Data were expressed as means ± SD (n = 3); [b] Sorafenib was used as a positive control.

In order to investigate the potential impact of compound **1** on HCC migration and invasion, the transwell assays showed that compound **1** dose-dependently decreased the numbers of migration and invasion in HepG2 cells. The effect of compound **1** on metastasis-related protein enhanced the expression level of E-cadherin, and decreased the expression of N-cadherin and Vimentin. These findings suggested that compound **1** effectively inhibited HCC cells migration and invasion *in vitro* (Figure 5).

The effect of compound **1** on cell cycle and apoptosis was performed by flow cytometry (FACS) to suggest compound **1** significantly induced the HepG2 cells arrest in G2/M phase in a concentration-dependent manner, and the percentage of cells in the G2/M phase increased from 21.8% to 24.1% (4.0 μmol/L), 30.9% (8.0 μmol/L) and 38.6% (12.0 μmol/L) independently (Figures 6A and B). Western blot showed that compound **1** suppressed the expression of pcdc2, and increased the expression of CyclinB1 (Figure 6C). These findings demonstrated that compound **1** had remarkable impact on cell cycle.

FACS data of the apoptosis effects on compound **1** showed an increase in apoptotic cells when the concentration of compound **1** increased from 11.1% (4.0 μmol/L) to 27.1% (8.0 μmol/L), and 66.2% (12.0 μmol/L) by contrast to the control cells (Figures 7A and 7B). Furthermore, compound **1** upregulated the expression of Bax, and downregulated the expression of Bcl-2 in line with the Western blot result. Overall, these finding suggested that compound **1** inhibited the proliferation in HepG2 cells through inducing cell apoptosis.

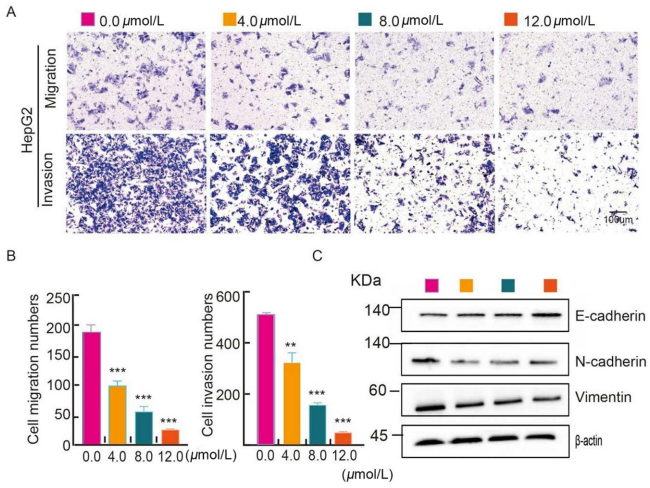

Figure 5 Compound **1** decreased the migration and invasion capacities of HepG2 cells. (A) Representative images of migration and invasion of HepG2 cells tested by Transwell assays. (B) Quantification data of migrated and invaded cells. (C) Transwell related proteins E-cadherin, N-cadherin and Vimentin were evaluated by Western blot. $^{**}P < 0.01$, $^{***}P < 0.001$, $n = 3$.

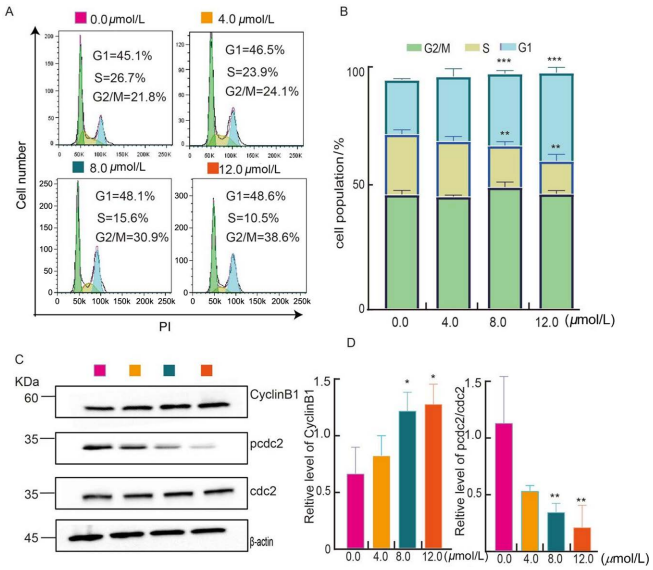

Figure 6 The effect of compound **1** (0.0, 4.0, 8.0 and 12.0 μmol/L) treatment on cell cycle. (A) and (B) Flow cytometric analysis and cell cycle quantification of HepG2 cells. (C) and (D) The cell cycle-associated protein levels in hepatoma cells treated with **1** for 12 h. Western blot and statistical results of CyclinB1, cdc2, pcdc2. $^{*}P < 0.05$, $^{**}P < 0.01$, and $^{***}P < 0.001$, $n = 3$.

Conclusions

In summary, the first connecting model of germacrane-guaiane (**1**—**3**) and eudesmane-guaiane (**4**—**6**) sesquiterpenoid dimers were isolated from *A. princeps* guided by bioactivity and elucidated by comprehensive spectral data and ECD calculation. Compounds **1**—**6** demonstrated cytotoxicity against three hepatoma cell lines with IC_{50} values in the range of 5.0—67.3 μmol/L. Importantly, compound **1** manifested significant cytotoxicity against HepG2, Huh7, and SK-Hep-1 cells with IC_{50} values of 9.9, 9.2, and 5.0 μmol/L, which were almost equivalent to the positive control, sorafenib. Mechanism investigation in HepG2 cells suggested the most active compound **1** dose-dependently inhibited cell migration and invasion, significantly induced G2/M cell cycle arrest by downregulating proteins pcdc2 and upregulating the

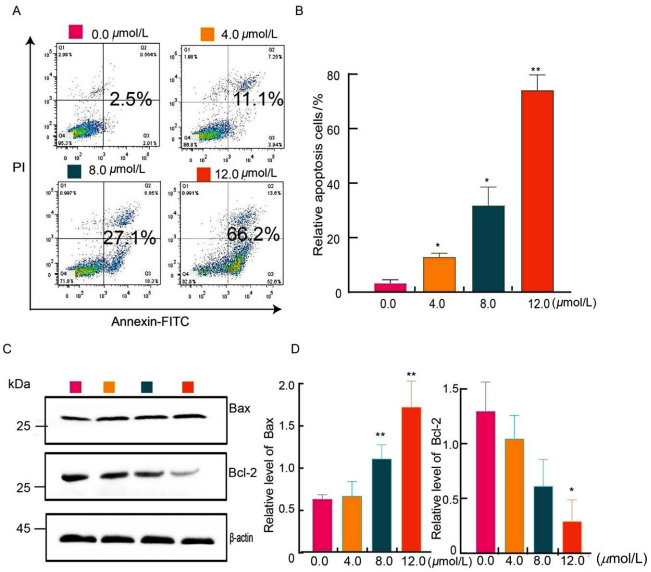

Figure 7 Compound **1** regulated HepG2 cells apoptosis by the Flow cytometric. (A) and (B) Flow cytometric analysis and cell apoptosis quantification of HepG2 cells. (C) and (D) The apoptosis-related protein levels in hepatoma cells treated with **1** for 48 h. Western blot and statistical results of Bax, Bcl-2. $^{*}P < 0.05$, $^{**}P < 0.01$, and $^{***}P < 0.001$, $n = 3$.

level of protein CyclinB1, and induced apoptosis by downregulating of Bcl-2 expression and upregulating Bax level. This investigation disclosed that compound **1** might be considered as a potent antihepatoma candidate, and laid a foundation for further systematic clarification of the pharmacological substances of *A. princeps*.

Experimental

General experimental instruments and procedures are provided in Supporting Information.

Plant material

The plant of *Artemisia princeps* Pamp. was collected from Hanzhong City of Shanxi Province, People's Republic of China in July 2020, and authenticated by Prof. Dr. Li-gong Lei (Kunming Institute of Botany, Chinese Academy of Sciences, CAS). A voucher specimen (No. 20200715-01) was deposited in the Laboratory of Antivirus and Natural Medicinal Chemistry, Kunming Institute of Botany, Chinese Academy of Sciences.

Extraction, isolation and purification of compounds

The air-dried stems and leaves of *A. princeps* (49.5 kg) were powered and extracted with 90% EtOH (200 L × 2, each for 3 d) at room temperature. The combined extracts were concentrated to remove the organic solvent, and further partitioned between H_2O and EtOAc. The EtOAc fraction (2.0 kg) was chromatographed on silica gel column chromatography (Si CC, 10 kg, 15 × 120 cm) and eluted with a gradient of acetone–petroleum ether (10 : 90 to 100 : 0, *V*/*V*) to afford five fractions, Fr. 1—Fr. 5 (867 g, 205 g, 147 g, 90 g, 415 g). Fr. 2 (205 g) was fractionated by MPLC on an MCI gel CHP 20P column (550 g, 5.5 × 50 cm) using an H_2O–MeOH gradient (50 : 50 to 0 : 100) to provide four subfractions, Fr. 2-1—Fr. 2-4. Fr. 2-3 (40 g) was separated on Si CC (400 g, 10 × 25 cm, EtOAc–PE, 20 : 80 to 100 : 0) to afford four subfractions (Fr. 2-3-1—Fr. 2-3-4). Fr. 2-3-3 (14.5 g) was separated into three subfractions (Fr. 2-3-3-1—Fr. 2-3-3-3) by MPLC on a RP-C18 column using a H_2O–MeOH gradient (40 : 60 to 0 : 100). The obtained Fr. 2-3-3-1 (2.1 g) was further purified by Sephadex LH-20 CC (140 g, 2.5 × 175 cm, MeOH–$CHCl_3$, 50 : 50) and preparative HPLC (H_2O–CH_3CN,

47 : 53, 10.0 mL/min) to yield compounds **2** (22 mg, t_R = 29.5 min) and **3** (25 mg, t_R = 30.2 min). Fr. 3 (147 g) was separated on an MCI gel CHP 20P column with H_2O–MeOH (50 : 50, 30 : 70, 10 : 90, and 0 : 100) as the mobile phase to provide four subfractions: Fr. 3-1—Fr. 3-4 (45 g, 26 g, 24.5 g, 48 g). Fr. 3-2 was fractionated by MPLC on a RP-C18 column using a H_2O–MeOH gradient (50 : 50 to 30 : 70) to give three subfractions (Fr. 3-2-1—Fr. 3-2-3). Separation of Fr. 3-2-2 (6.5 g) by MPLC on a RP-C18 column using a H_2O–CH_3CN gradient (70 : 30 to 50 : 50) gave five subfractions (Fr. 3-2-2-1—Fr. 3-2-2-5). Further separation of Fr. 3-2-2-2 (1.7 g) by preparative HPLC (H_2O–MeCN, 60 : 40, 10.0 mL/min) afforded five subfractions (Fr. 3-2-2-2a—Fr. 3-2-2-2e). The obtained Fr. 3-2-2-2b (223 mg) was purified by semipreparative HPLC on a XBridge® Prep OBD™ C18 column (H_2O–MeOH, 42 : 58, 3.0 mL/min) to produce compound **1** (5 mg, t_R = 22.5 min). Similarly, compound **4** (5 mg, t_R = 30.8 min) was obtained from Fr. 3-2-2-2c (37 mg) through semipreparative HPLC on an Eclipse XDB-C18 column (H_2O–MeCN, 62 : 38, 3.0 mL/min). The obtained Fr. 3-2-2-2d (337 mg) was separated into four subfractions (Fr. 3-2-2-2d-1—Fr. 3-2-2-2d-4) by semipreparative HPLC on an Eclipse XDB-C18 column (H_2O–MeCN, 62 : 38, 3.0 mL/min). From Fr. 3-2-2-2d-4 (21 mg), compounds **5** (10 mg, t_R = 16.2 min) and **6** (3 mg, t_R = 18.3 min) were purified by semipreparative HPLC on an Opti-Chiral C1-5R column using H_2O–MeCN (58 : 42, 3.0 mL/min).

Spectroscopic data of compounds

Artemiprincepsolide A (**1**): white amorphous powder; $[\alpha]_D^{21}$ +38.0 (*c* 0.10, MeOH); ECD (MeOH) λ_{max} ($\Delta\varepsilon$): 203 (+0.11), 219 (+14.58), 244 (–0.41) nm; IR ν_{max}: 3495, 1764, 1712, 1632, 1401, 1290, 1126 cm^{-1}; ^1H and ^{13}C NMR data, see Tables 1 and 2; (–)-HRESIMS *m/z* 539.2659 $[M + HCOO]^-$ (calcd for $C_{31}H_{39}O_8$, 539.2650).

Artemiprincepsolide B (**2**): white amorphous powder; $[\alpha]_D^{23}$ +26.6 (*c* 0.07, MeOH); ECD (MeOH) λ_{max} ($\Delta\varepsilon$): 201 (–1.89), 219 (+8.52), 244 (–0.65) nm; IR ν_{max}: 3436, 1763, 1630, 1400, 1298, 1263, 1077 cm^{-1}; ^1H and ^{13}C NMR data, see Tables 1 and 2; (–)-HRESIMS *m/z* 581.2734 $[M + HCOO]^-$ (calcd for $C_{33}H_{41}O_9$, 581.2756).

Artemiprincepsolide C (**3**): white amorphous powder; $[\alpha]_D^{27}$ −16.9 (*c* 0.13, MeOH); ECD (MeOH) λ_{max} ($\Delta\varepsilon$): 200 (–4.92), 212 (+7.29), 232 (–4.09) nm; IR ν_{max}: 3436, 1765, 1631, 1457, 1386, 1265, 1155, 1058 cm^{-1}; ^1H and ^{13}C NMR data, see Tables 1 and 2; (–)-HRESIMS *m/z* 581.2751 $[M + HCOO]^-$ (calcd for $C_{33}H_{41}O_9$, 581.2756).

Artemiprincepsolide D (**4**): white amorphous powder; $[\alpha]_D^{20}$ +0.7 (*c* 0.11, MeOH); ECD (MeOH) λ_{max} ($\Delta\varepsilon$): 196 (+11.32), 240 (–0.75), 289 (+0.98) nm; IR ν_{max}: 3447, 1766, 1714, 1643, 1379, 1356, 1153 cm^{-1}; ^1H and ^{13}C NMR data, see Tables 1 and 2; (–)-HRESIMS *m/z* 555.2606 $[M + HCOO]^-$ (calcd for $C_{31}H_{39}O_9$, 555.2600).

Artemiprincepsolide E (**5**): white amorphous powder; $[\alpha]_D^{28}$ +29.9 (*c* 0.04, MeOH); ECD (MeOH) λ_{max} ($\Delta\varepsilon$): 195 (+10.80), 252 (–0.91), 297 (+0.25), 301 (+0.21) nm; IR ν_{max}: 3468, 1754, 1631, 1458, 1380, 1254, 1216, 1053 cm^{-1}; ^1H and ^{13}C NMR data, see Tables 1 and 2; (–)-HRESIMS *m/z* 597.2491 $[M + HCOO]^-$ (calcd for $C_{33}H_{41}O_{10}$, 597.2494).

Artemiprincepsolide F (**6**): white amorphous powder; $[\alpha]_D^{28}$ +25.8 (*c* 0.12, MeOH); ECD (MeOH) λ_{max} ($\Delta\varepsilon$): 195 (+10.46), 208 (–8.88), 233 (+0.60), 256 (–0.45), nm; IR ν_{max}: 3435, 1763, 1631, 1456, 1378, 1243, 1177, 1088 cm^{-1}; ^1H and ^{13}C NMR data, see Tables 1 and 2; (–)-HRESIMS *m/z* 597.2708 $[M + HCOO]^-$ (calcd for $C_{33}H_{41}O_{10}$, 597.2705).

MTT assay

The cytotoxicities of all the isolates were assayed by MTT method on three human hepatocellular carcinoma cell lines (HepG2, Huh7, and SK-Hep-1).[23] The cells were harvested and seeded in a 96-well plate at a density of 9 × 10^3 cells per well. After incubating the cells with 5% CO_2 at 37 °C for 24 h, samples with different concentrations (200, 100, 50, 25, 12.5, 6.25, 3.125 μmol/L) were added to cells and incubated for 48 h. Thereafter, 100 μL of MTT solution (1 mg/mL) was added into each well and co-incubated for 4 h at 37 °C. Then the solution was removed, and 100 μL of dimethyl sulfoxide (DMSO) was added to dissolve the MTT formazan salt. Finally, the optical density (OD) was recorded at 490 nm using a microplate reader (BIO-RAD, USA). The inhibitory ratios were calculated as $[A_{(control)} - A_{(sample)}] / A_{(control)} \times 100\%$, and IC_{50} values were calculated by GraphPad Prism 7 (GraphPad Software, San Diego, CA, USA). All results and data were expressed as mean ± SD at three independent experiments.

Cell migration and invasion assays

Transwell assays were used to examine the migration and invasion of HepG2 cells (Corning, USA). HepG2 cells (10 × 10^5 cells/mL) were seeded on the upper chambers. After adherence, the cells were maintained in serum-free DMEM with various concentrations of compound **1** for 48 h. Then, cells in the upper chambers were wiped, and the migrated cells were fixed in 70% ethanol and stained with crystal violet solution (0.1%) for 30 min. After that, images were taken by imaging system (Olympus IX73). For cell invasion assay, the difference is matrigel (BD Biosciences) that was diluted to 1 : 50 in pre-cool DMEM medium and added to the upper chamber 2 h prior to seeding the cells.[23]

Flow cytometry assays

We assessed the effect of compound **1** on cell cycle and apoptosis by flow cytometry. HepG2 cells were seeded into 6-well plates at a density of 3 × 10^5 cells per well. Then, cells were treated with various concentrations (0.0, 4.0, 8.0 and 12.0 μmol/L) of compound **1** for 12 h (cell cycle) or 48 h (apoptosis). In cell cycle assay, cells were collected and fixed in 70% ethanol at –20 °C overnight. Thereafter, HepG2 cells were resuspended in PBS containing in staining buffer of 100 μg/mL PI and 200 μg/mL RNase A. In apoptosis assay, cells were suspended in binding buffer, and stained with fluorochrome Annexin V/PI for 15 min. Finally, the cells were analyzed by flow cytometry by using a BD AccuriC6 flow cytometer (BD Biosciences, San Jose, CA, USA).[23]

Western blot

The expression of apoptosis and cell cycle-related proteins was evaluated by Western blot. HepG2 cells were seeded into 6-well plates and treated with compound **1** for 48 h. The cells were collected and lysed in RIPA buffer to extract total protein, and the BCA assay determined the protein concentration. Samples were fractionated using SDS-PAGE and transferred to PVDF membranes. Then, the membranes were incubated with specific primary antibodies at 4 °C overnight. The secondary antibody was incubated for 2 h at room temperature. Proteins were detected by ECL solution (Tanon) and photographed by the multispectral imaging system (sage creation).[23]

Theoretical ECD calculations for compounds 1—6

The ECD spectra of compounds **1**—**6** were calculated using Gaussian 09 software. The relative configurations of those compounds were determined based on their ROESY experiments and optimized by DFT calculation at the b3lyp/6-31G(d,p) level in gas phase. In order to exclude imaginary frequencies, frequency calculations were performed at the same level. ECD calculations were performed using the TDDFT methodology at the b3lyp/6-31G(d,p) level with the consideration of solvent effects. The ECD curves were drawn using the Origin Pro 9 program (OriginLab Corporation, Northampton, MA, USA).

Supporting Information

The supporting information for this article is available on the WWW under https://doi.org/10.1002/cjoc.202300242.

Acknowledgement

This work was financially supported by the Key Program of the National Natural Science Foundation of China (22137008), the Xingdian Yingcai Project (YNWR-KJLJ-2019-002), the Youth Innovation Promotion Association, CAS (2020386), the Reserve Talents of Young and Middle-aged Academic and Technical Leaders in Yunnan Province (202105AC160021).

References

[1] Llovet, J. M.; Kelley, R. K.; Villanueva, A.; Singal, A. G.; Pikarsky, E.; Roayaie, S.; Lencioni, R.; Koike, K.; Zucman-Rossi, J.; Finn, R. S. Hepatocellular carcinoma. *Nat. Rev. Dis. Primers* **2021**, *7*, 28.

[2] Sangro, B.; Sarobe, P.; Hervás-Stubbs, S.; Melero, I. Advances in immunotherapy for hepatocellular carcinoma. *Nat. Rev. Gastroenterol. Hepatol.* **2021**, *18*, 525–543.

[3] Khan, A. A.; Liu, Z.-k.; Xu, X. Recent advances in immunotherapy for hepatocellular carcinoma. *Hepatobiliary Pancreatic Dis. Int.* **2021**, *20*, 511–520.

[4] Bonilla, C. M.; McGrath, N. A.; Fu, J. Y.; Xie, C. Q. Immunotherapy of hepatocellular carcinoma with infection of hepatitis B or C virus. *Hepatoma Res.* **2020**, *6*, 1–14.

[5] Ho, W. J.; Zhu, Q.; Durham, J.; Popovic, A.; Xavier, S.; Leatherman, J.; Mohan, A.; Mo, G.; Zhang, S.; Gross, N.; Charmsaz, S.; Lin, D.; Quong, D.; Wilt, B.; Kamel, I. R.; Weiss, M.; Philosophe, B.; Burkhart, R.; Burns, W. R.; Shubert, C.; Ejaz, A.; He, J.; Deshpande, A.; Danilova, L.; Stein-O'Brien, G.; Sugar, E. A.; Laheru, D. A.; Anders, R. A.; Fertig, E. J.; Jaffee, E. M.; Yarchoan, M. Neoadjuvant cabozantinib and nivolumab convert locally advanced hepatocellular carcinoma into resectable disease with enhanced antitumor immunity. *Nat. Cancer* **2021**, *2*, 891–903.

[6] Zhan, Z. J.; Ying, Y. M.; Ma, L. F.; Shan, W. G. Natural disesquiterpenoids. *Nat. Prod. Rep.* **2011**, *28*, 594–629.

[7] Ma, L. F.; Chen, Y. L.; Shan, W. G.; Zhan, Z. J. Natural disesquiterpenoids: an update. *Nat. Prod. Rep.* **2020**, *37*, 999–1030.

[8] Li, Y. T.; Li, S. F.; Lei, C.; You, J. Q.; Huang, J. C.; Hou, A. J. Dimeric sesquiterpenoids and anti-inflammatory constituents of *Sarcandra glabra*. *Bioorg. Chem.* **2022**, *124*, 105821.

[9] Li, A.; Jiao, S. G.; Huang, H. M.; Chen, P. L.; Zhang, R. F.; Su, G. Z.; Xu, J. X.; Liu, C. X.; Hu, Z. D.; Chen, S.; Tu, P. F.; Chai, X. Y.; Huang, L. Q. Syringenes A–L: bioactive dimeric eremophilane sesquiterpenoids from *Syringa pinnatifolia*. *Bioorg. Chem.* **2022**, *125*, 105879.

[10] Qin, D. P.; Pan, D. B.; Xiao, W.; Li, H. B.; Yang, B.; Yao, X. J.; Dai, Y.; Yu, Y.; Yao, X. S. Dimeric cadinane sesquiterpenoid derivatives from *Artemisia annua*. *Org. Lett.* **2018**, *20*, 453–456.

[11] Zhang, C.; Wen, R.; Ma, X. L.; Zeng, K. W.; Xue, Y.; Zhang, P. M.; Zhao, M. B.; Jiang, Y.; Liu, G. Q.; Tu, P. F. Nitric oxide inhibitory sesquiterpenoids and its dimers from *Artemisia freyniana*. *J. Nat. Prod.* **2018**, *81*, 866–878.

[12] Zhou, M.; Duan, F. F.; Gao, Y.; Peng, X. G.; Meng, X. G.; Ruan, H. L. Eremophilane sesquiterpenoids from the whole plant of *Parasenecio albus* with immunosuppressive activity. *Bioorg. Chem.* **2021**, *115*, 105247.

[13] Min, S. W.; Kim, N. J.; Baek, N. I.; Kim, D. H. Inhibitory effect of eupatilin and jaceosidin isolated from *Artemisia princeps* on carrageenan-induced inflammation in mice. *J. Ethnopharmacol.* **2009**, *125*, 497–500.

[14] Zhang, J.; Sasaki, T.; Li, W.; Nagata, K.; Higai, K.; Feng, F.; Wang, J.; Cheng, M. S.; Koike, K. Identification of caffeoylquinic acid derivatives as natural protein tyrosine phosphatase 1B inhibitors from *Artemisia princeps*. *Bioorg. Med. Chem. Lett.* **2018**, *28*, 1194–1197.

[15] Akihisa, T.; Kawashima, K.; Orido, M.; Akazawa, H.; Matsumoto, M.; Yamamoto, A.; Ogihara, E.; Fukatsu, M.; Tokuda, H.; Fuji, J. Antioxidative and melanogenesis-inhibitory activities of caffeoylquinic acids and other compounds from *Moxa*. *Chem. Biodiversity* **2013**, *10*, 313–327.

[16] Lee, T. H.; Jung, H.; Park, K. H.; Bang, M. H.; Baek, N. I.; Kim, J. Y. Jaceosidin, a natural flavone, promotes angiogenesis *via* activation of VEGFR2/FAK/PI3K/AKT/NF-κB signaling pathways in endothelial cells. *Exp. Biol. Med.* **2014**, *239*, 1325.

[17] Yano, K.; Takahashi, S.; Furukawa, T. Polyacetylene compounds from Japanese mugwort. *Phytochemistry* **1972**, *11*, 2577–2579.

[18] Yamada, H.; Ohtani, K.; Kiyohara, H.; Cyong, J. C.; Otsuka, Y.; Ueno, Y.; Omura, S. Purification and chemical properties of anti-complementary polysaccharide from the leaves of *Artemisia princeps*. *Planta Med.* **1985**, 121–125.

[19] Yamada, H.; Otsuka, Y.; Omura, S. Structural characterization of anti-complementary polysaccharides from the leaves of *Artemisia princeps*. *Planta Med.* **1986**, 311–314.

[20] Yano, K.; Nishijima, T. Sesquiterpenes from *Artemisia princeps*. *Phytochemistry* **1974**, *13*, 1207–1208.

[21] Ryu, S. Y.; Kim, J. O.; Choi, S. U. Cytotoxic components of *Artemisia princeps*. *Planta Med.* **1997**, *63*, 384–385.

[22] Bang, M. H.; Han, M. W.; Song, M. C.; Cho, J. G.; Chung, H. G.; Jeong, T. S.; Lee, K. T.; Choi, M. S.; Kim, S. Y.; Baek, N. I. A cytotoxic and apoptosis-inducing sesquiterpenoid isolated from the aerial parts of *Artemisia princeps* Pampanini *Chem. Pharm. Bull.* **2008**, *56*, 1168–1172.

[23] Su, L. H.; Zhang, X. T.; Ma, Y. B.; Geng, C. A.; Huang, X. Y.; Hu, J.; Li, T. Z.; Tang, S.; Shen, C.; Gao, Z.; Zhang, X. M.; Chen, J. J. New guaiane-type sesquiterpenoid dimers from *Artemisia atrovirens* and their antihepatoma activity. *Acta Pharm. Sin. B* **2021**, *11*, 1648–1666.

[24] Su, L. H.; Li, T. Z.; Geng, C. A.; Ma, Y. B.; Huang, X. Y.; Wang, J. P.; Zhang, X. M.; Chen, J. J. Trimeric and dimeric sesquiterpenoids from *Artemisia atrovirens* and their cytotoxicities. *Org. Chem. Front.* **2021**, *8*, 1249–1256.

[25] Su, L. H.; Li, T. Z.; Ma, Y. B.; Geng, C. A.; Huang, X. Y.; Zhang, X.; Gao, Z.; Chen, J. J. Artematrovirenolides A–D and Artematrolides S–Z, sesquiterpenoid dimers with cytotoxicity against three hepatoma cell lines from *Artemisia atrovirens*. *Chin. J. Chem.* **2022**, *40*, 104–114.

[26] Gao, Z.; Ma, W. J.; Li, T. Z.; Ma, Y. B.; Hu, J.; Huang, X. Y.; Geng, C. A.; He, X. F.; Zhang, X. M.; Chen, J. J. Artemidubolides A–T, cytotoxic unreported guaiane-type sesquiterpenoid dimers against three hepatoma cell lines from *Artemisia dubia*. *Phytochemistry* **2022**, *202*, 113299.

[27] Zhang, X. T.; Hu, J.; Su, L. H.; Geng, C. A.; Chen, J. J. Artematrolide A inhibited cervical cancer cell proliferation via ROS/ERK/mTOR pathway and metabolic shift. *Phytomedicine* **2021**, *91*, 153707.

[28] He, X. F.; Ma, W. J.; Hu, J.; Li, T. Z.; Geng, C. A.; Ma, Y. B.; Wang, M. F.; Yang, K. X.; Zhang, X. M.; Chen, J. J. Diverse structures and antihepatoma effect of sesquiterpenoid dimers from *Artemisia eriopoda* by AKT/STAT signaling pathway. *Signal Transduct. Tar.* **2023**, *8*, 64–66.

[29] Xue, G. M.; Li, X. Q.; Chen, C.; Chen, K.; Wang, X. B.; Gu, Y. C.; Luo, J. G.; Kong, L. Y. Highly oxidized guaianolide sesquiterpenoids with potential anti-inflammatory activity from *Chrysanthemum indicum*. *J. Nat. Prod.* **2018**, *81*, 378–386.

[30] Pyee, Y.; Chung, H. J.; Choi, T. J.; Park, H. J.; Hong, J. Y.; Kim, J. S.; Kang, S. S.; Lee, S. K. Suppression of inflammatory responses by handelin, a guaianolide dimer from *Chrysanthemum boreale*, via downregulation of NF-κB signaling and pro-inflammatory cytokine production. *J. Nat. Prod.* **2014**, *77*, 917–924.

[31] Tarasov, V. A.; Abdullaev, N. D.; Kasymov, S. Z.; Sidyakin, G. P. Hanphyllin, a new germacranolide from *Handelia trichophylla*. *Khim. Prir. Soedin.* **1976**, 2, 263–264.

[32] Tang, S.; Zhang, X. T.; Ma, Y. B.; Huang, X. Y.; Geng, C. A.; Li, T. Z.; Zhang, X. M.; Shen, C.; Su, L. H.; Gao, Z.; Chen, J. J. Artemyrianolides A–S, cytotoxic sesquiterpenoids from *Artemisia myriantha*. *J. Nat. Prod.* **2020**, *83*, 2618–2630.

[33] Shen, C.; Huang, X. Y.; Geng, C. A.; Li, T. Z.; Wang, J. P.; Tang, S.; Su, L. H.; Gao, Z.; Zhang, X. M.; Chen, J. J. Cytotoxic sesquiterpenoids against hepatic stellate cell line LX2 from *Artemisia lavandulaefolia*. *Bioorg. Chem.* **2020**, *103*, 104107.

[34] Wen, J.; Shi, H. M.; Xu, Z. R.; Chang, H. T.; Jia, C. Q.; Zan, K.; Jiang, Y.; Tu, P. F. Dimeric guaianolides and sesquiterpenoids from *Artemisia anomala*. *J. Nat. Prod.* **2010**, *73*, 67–70.

Manuscript received: April 26, 2023
Manuscript revised: June 6, 2023
Manuscript accepted: June 7, 2023
Accepted manuscript online: June 10, 2023
Version of record online: July 19, 2023

The Authors

Left to Right: Li-Hua Su, Wen-Jing Ma, Yun-Bao Ma, Tian-Ze Li, Chang-An Geng, Wei Dong, Xiao-Feng He, Xue-Mei Zhang, and Ji-Jun Chen